Top quark mass effects in $gg \to ZZ$ at two loops and off-shell Higgs boson interference

Ramona Gröber,[1,2,*] Andreas Maier,[3,†] and Thomas Rauh[4,‡]

[1]*Institut für Physik, Humboldt-Universität zu Berlin, 12489 Berlin, Germany*
[2]*Dipartimento di Fisica e Astronomia "G. Galilei", Università di Padova, and Istituto Nazionale di Fisica Nucleare, Sezione di Padova, I-35131 Padova, Italy*
[3]*Deutsches Elektronen–Synchrotron, DESY, Platanenallee 6, D–15738 Zeuthen, Germany*
[4]*Albert Einstein Center for Fundamental Physics, Institute for Theoretical Physics, University of Bern, Sidlerstrasse 5, CH-3012 Bern, Switzerland*

(Received 22 August 2019; published 10 December 2019)

We consider top-quark mass effects in the Higgs-interference contribution to Z-boson pair production in gluon fusion. While this production mechanism is formally of next-to-next-to leading order, its contribution is numerically important above the top threshold $M_{ZZ}^2 = 4m_t^2$. This region is essential to constrain the width of the Higgs boson, and good control over the top-quark mass dependence is crucial. We determine the form factors that are relevant for the interference contribution at two-loop order using a method based on a conformal mapping and Padé approximants constructed from the expansions of the amplitude for large top mass and around the top threshold.

DOI: 10.1103/PhysRevD.100.114013

I. INTRODUCTION

A direct measurement of the Higgs boson width Γ_H is not possible at the LHC or even the envisioned next generation of collider experiments. However, indirect constraints can be obtained at the LHC by studying the process $pp \to H \to ZZ(\to 4l)$ on the Higgs boson peak where the cross section depends on the combination $g_{Hgg}^2 g_{HZZ}^2/\Gamma_H$ and off the peak where the measurement of the cross section constrains the product $g_{Hgg}^2 g_{HZZ}^2$ of the effective Higgs boson-gluon coupling g_{Hgg} and the Higgs boson-Z boson coupling g_{HZZ}, as proposed in [1–3].[1] The same strategy can be employed with WW final states [6]. The latest studies from the LHC experiments give an upper limit of 14.4 MeV at 95% C.L. from the ZZ final state at ATLAS [7] and the value $3.2^{+2.8}_{-2.2}$ MeV from the combination of VV final states in CMS [8], close to the SM prediction $\Gamma_H^{\mathrm{SM}} = 4.10 \pm 0.06$ MeV [9]. Measurements of the Higgs boson signal at large invariant mass can also be used to directly constrain physics beyond the Standard Model in the Higgs sector [10–13].

Here, we focus on the loop-induced continuum gluon fusion process $gg \to ZZ$ and in particular its interference with the off-shell Higgs contribution $gg \to H^* \to ZZ$. Despite the narrow width of the Higgs boson, these interference effects are sizable with 10% of the Higgs signal stemming from the off-shell region where the invariant mass of the two decay products is greater than $2m_Z$ [1] and higher-order corrections are required to control the uncertainties. The Higgs-mediated amplitude only depends on two scales, the mass m_q of the quark in the loop and the invariant mass M_{ZZ} of the final state. Next-to-leading order (NLO) corrections with the full quark-mass dependence have been known for some time [14–17], and the top-quark mass dependence at next-to-next-to leading order has been reconstructed very recently [18] (see also [19]). On the other hand, the continuum amplitude depends on four scales m_q, m_Z, M_{ZZ}, and the transverse momentum p_T of one of the Z bosons, and the exact result is only known at leading order (LO) [20] while an analytic NLO calculation appears extremely challenging. In the massless limit $m_q = 0$, the two-loop amplitude has been determined in [21–23] and the NLO cross section in [24]. Recently, also the quark-gluon channel has been included [25].

The contribution from top quarks at two-loop order has been computed in a large-mass expansion (LME) [24,26,27] and is known up to $1/m_t^{12}$. While the contribution from massless quarks dominates the interference correction at small invariant masses, the top-quark

*ramona.groeber@physik.hu-berlin.de
†andreas.martin.maier@desy.de
‡rauh@itp.unibe.ch

[1]Note that the indirect way of constraining the Higgs width is not entirely model-independent [4,5].

contribution is of the same size near the top threshold $M_{ZZ} = 4m_t^2$ and dominates in the large invariant-mass regime. Since the LME ceases to provide a reliable description above the top threshold, the authors of [27] have improved their prediction by a conformal mapping and the construction of Padé approximants based on the available number of LME coefficients. In [28], we have extended this method by considering the expansion around the top threshold in addition to the LME and demonstrated that the top-mass effects can be reproduced correctly by comparing results for the two-loop amplitude for $gg \to HH$ with the numerical calculation performed in Refs. [29–31].[2]

In this work, we consider the form factors of the continuum $gg \to ZZ$ amplitude that are relevant for the interference contribution at one and two loops. The nonanalytic terms in the expansion around the top threshold are computed up to at least order $(1-z)^4$, where $z = M_{ZZ}^2/(4m_t^2) + i0$, and used to construct Padé approximants. Together with the exactly known real NLO top quark [27,38] and the massless quark corrections [21–25], this is sufficient to determine the full NLO interference contribution with realistic top-quark mass dependence.

II. FORM FACTORS FOR INTERFERENCE

Up to the two-loop level, the amplitude for the top-mediated nonresonant continuum production process $g(\mu, A, p_1) + g(\nu, B, p_2) \to Z(\alpha, p_3) + Z(\beta, p_4)$ receives contributions from both box and double-triangle diagrams; see Fig. 1. The latter are known for arbitrary quark masses [27,39] and will not be discussed in the following.

The box amplitude $|B^{AB}_{\mu\nu\alpha\beta}\rangle$ has a complicated tensor structure [20–22,40]. However, the interference with the Higgs-mediated amplitude is described by a single form factor. Adopting the conventions of [27], it takes the form

$$|\mathcal{B}\rangle = \frac{\delta^{AB}}{N_A}(p_1\cdot p_2 g^{\mu\nu} - p_1^\nu p_2^\mu) P_Z^{\alpha\rho}(p_3) P_{Z,\rho}^{\beta}(p_4)|B^{AB}_{\mu\nu\alpha\beta}\rangle, \tag{1}$$

with $N_A = N_c^2 - 1$ and $P_Z^{\alpha\rho}(p) = -g^{\alpha\rho} + p^\alpha p^\rho/m_Z^2$. The form factor can be decomposed into a vector and axial-vector part

$$|\mathcal{B}\rangle = \frac{ig_W^2}{4\cos^2\theta_W}(v_t^2|\tilde{\mathcal{B}}_{VV}\rangle + a_t^2|\tilde{\mathcal{B}}_{AA}\rangle), \tag{2}$$

where $a_t = 1/2$ and $v_t = 1/2 - 4/3\sin^2\theta_W$ denote the axial-vector and vector couplings for an up-type quark. Mixed $v_t a_t$ terms are forbidden by charge conjugation symmetry. The order in the strong coupling constant α_s is indicated as follows:

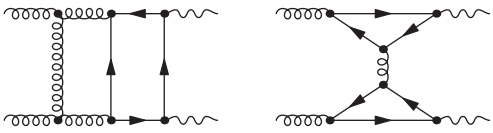

FIG. 1. Examples for box (left) and double-triangle (right) top-mediated contributions to $gg \to ZZ$.

$$|\tilde{\mathcal{B}}_i\rangle = \frac{\alpha_s}{4\pi}|\tilde{\mathcal{B}}_i^{(1)}\rangle + \left(\frac{\alpha_s}{4\pi}\right)^2|\tilde{\mathcal{B}}_i^{(2)}\rangle + \ldots, \tag{3}$$

with $i = VV, AA$. At order α_s^2, the renormalized form factors contain IR divergences, which cancel in the combination with real corrections, and we define the finite remainder by applying the subtraction [41][3]

$$|\tilde{\mathcal{F}}_i^{(2)}\rangle = |\tilde{\mathcal{B}}_i^{(2)}\rangle + \frac{e^{\epsilon\gamma_E}}{\Gamma(1-\epsilon)}\left[\frac{2C_A}{\epsilon^2}\left(\frac{\mu^2}{-s}\right)^\epsilon + \frac{\beta_0}{\epsilon}\right]|\tilde{\mathcal{B}}_i^{(1)}\rangle, \tag{4}$$

where $\beta_0 = \frac{11}{3}C_A - \frac{4}{3}T_f n_l, C_A = 3, T_f = \frac{1}{2}, n_l = 5$, and the form factors $|\tilde{\mathcal{B}}_i^{(1,2)}\rangle$ are defined in $d = 4 - 2\epsilon$ dimensions. The one-loop form-factors $|\tilde{\mathcal{B}}_i^{(1)}\rangle$ are already finite; we define $|\tilde{\mathcal{F}}_i^{(1)}\rangle = |\tilde{\mathcal{B}}_i^{(1)}\rangle$ for the sake of a consistent notation.

A. The amplitude near threshold

Above the top threshold at $z = 1$, the top quarks in the loop can go on shell which manifests as nonanalytic terms in the expansion of the form factors in $\bar{z} \equiv 1 - z$, generating a sizable imaginary part. As shown in [28], the knowledge of these terms alone provides very valuable information for the determination of top-quark mass effects in our approach. The calculation of the nonanalytic terms is significantly simpler than that of the analytic contributions and was described in detail in [28] for the three leading nonanalytic expansion terms of the one- and two-loop form factors for $gg \to HH$. For $gg \to ZZ$, we expand the amplitude up to high orders in $\bar{z} \equiv 1 - z$ and therefore use the expansion by regions [42,43] to expand the full-theory diagrams instead of an effective field theory approach where a large number of effective vertices is required due to the deep expansion. We use QGRAF [44] to generate the Feynman diagrams which are processed and expanded using private FORM [45] code. The integration-by-parts reduction [46] is performed with FIRE [47] which is based on the Laporta algorithm [48].

Our results are given in Appendix A and an ancillary Mathematica file [49]. They are of the form

$$|\tilde{\mathcal{F}}_i^{(1)}\rangle \overset{z\to 1}{\asymp} \sum_{n=3}^{\infty} a_i^{(n,0)}\bar{z}^{\frac{n}{2}},$$
$$|\tilde{\mathcal{F}}_i^{(2)}\rangle \overset{z\to 1}{\asymp} \sum_{n=2}^{\infty}\sum_{m=\bar{n}_2}^{1}[b_i^{(n,m)} + b_{i,\ln}^{(n,m)}\ln(-4z)]\bar{z}^{\frac{n}{2}}\ln^m\bar{z}, \tag{5}$$

[2]Recently, an independent numerical calculation [32], several approximations [33–36] which are consistent with the earlier results and a combined result [37] have appeared.

[3]Note that this subtraction differs at order ϵ^0 from the one given in Eq. (2.14) of [27].

where $\bar{n}_2$ is n modulo 2, the coefficients are functions of the dimensionless variables $r_Z = m_Z^2/M_{ZZ}^2$ and $\tilde{x} = (p_T^2 + m_Z^2)/M_{ZZ}^2$. We use the symbol $\asymp$ to indicate that terms which are analytic in $\bar{z}$ and currently unknown have been dropped on the right-hand side.

Threshold logarithms $\ln \bar{z}$ and logarithms $\ln(-4z)$ related to massless cuts in the amplitude first appear at two-loop order. While we generally compute the expansion coefficients up to $n = 8$, i.e., expand up to $\bar{z}^4$, we find that for the massless-cut contribution proportional to $\ln(-4z)$ more input is required to achieve a reliable Padé approximation. We therefore compute the corresponding coefficients $b_{i,\ln}^{(n,m)}$ up to $n = 9$.

As in Higgs pair production, there is no S-wave contribution to the form factors relevant for the interference and the leading nonanalytic terms involve the $\bar{z}$-suppressed P-wave Green function [50].

B. Behavior for $z \to \infty$

In addition to the LME and threshold expansions, we can exploit scaling information in the small-mass limit $m_t \to 0$ which corresponds to $z \to \infty$. This does not require an additional calculation in this region but relies solely on the symmetries of QCD. The absence of infrared $1/m_t$ power divergences as $m_t \to 0$ implies that the form factors can only show logarithmic behavior as $z \to \infty$. Below we show that the difference

$$|\tilde{\mathcal{B}}_{AA-VV}\rangle \equiv |\tilde{\mathcal{B}}_{AA}\rangle - |\tilde{\mathcal{B}}_{VV}\rangle \tag{6}$$

vanishes as $z \to \infty$. To prove this, we note that chirality is conserved in massless QCD and hence the four-point correlator of two vector currents, a left-handed and a right-handed current, which we denote in short by [V,V,V-A,V+A], vanishes in the limit of zero quark masses.[4] Using that the correlator [V,V,V,A] vanishes due to charge conjugation, we immediately conclude that [V,V,V,V]-$[\mathrm{V},\mathrm{V},\mathrm{A},\mathrm{A}] \to 0$ as $z \to \infty$. We exploit this below and reconstruct the top-mass dependence of $|\tilde{\mathcal{F}}_{VV}^{(i)}\rangle$ and $|\tilde{\mathcal{F}}_{AA}^{(i)}\rangle - |\tilde{\mathcal{F}}_{VV}^{(i)}\rangle$ where we have one additional condition for the latter.

III. THE METHOD

We approximate the box form factors (2) using our approach from [28]. First, we introduce subtraction functions $s_{VV}^{(2)}, s_{AA}^{(2)}$ in such a way that the combinations $|\tilde{\mathcal{F}}_i^{(2)}\rangle - s_i^{(2)}$ retain their analytic structure for $|z| < 1$ but have threshold expansions which are free of logarithms $\ln(\bar{z})$ up to the highest known order, i.e., up to $\bar{z}^4$. The construction of such subtraction functions is detailed in [28], and we give the ones we explicitly need in Appendix B. Note that even after this subtraction the threshold and large mass expansions of the two-loop form factors still receive contributions proportional to a single logarithm $L_s \equiv \ln(-4z)$ from diagrams with massless cuts. We therefore split the subtracted two-loop form factors into a constant and a logarithmic part and construct separate approximants for each part.

The top mass dependence is contained in the variable z and the conformal transformation [51]

$$z = \frac{4\omega}{(1+\omega)^2} \tag{7}$$

is used to map the entire complex z plane onto the unit disc $|\omega| \leq 1$. The physical branch cut for $z \geq 1$ corresponds to the perimeter of this disc. Further cuts arise outside the physical region for $z \leq \frac{s}{t}$ and $z \leq \frac{s}{u}$, where s, t, u are the usual partonic Mandelstam invariants. These cuts are mapped onto negative values of ω.

We then reconstruct the logarithmic and nonlogarithmic parts of the form factors using Padé approximants

$$[n/m](\omega) = \frac{\sum_{i=0}^{n} a_i \omega^i}{1 + \sum_{j=1}^{m} b_j \omega^j}, \tag{8}$$

where the $n + m + 1$ coefficients a_i, b_j can be fixed by imposing the condition that the expansion of Eq. (8) in the LME and threshold region must reproduce the known coefficients for given, fixed values of r_Z and $\tilde{x}$. The small-mass behavior discussed in Sec. II B is not used to further constrain the Padé coefficients, but is taken into account by a rescaling of the Padé ansatz. Hence, we use approximation functions of the form

$$\begin{aligned}
P_{AA-VV}^{(1)}(\omega) &= \frac{[n/m](\omega)}{1 + a_{R,0} z(\omega)}, \\
P_{AA-VV}^{(2)}(\omega) &= \frac{[n/m](\omega)}{1 + a_{R,0} z(\omega)} + \frac{[k/l](\omega)}{1 + a_{R,1} z(\omega)} L_s \\
&\quad + s_{AA}^{(2)}(z(w)) - s_{VV}^{(2)}(z(w)), \\
P_{VV}^{(1)}(\omega) &= \frac{z(\omega)[n/m](\omega)}{1 + a_{R,0} z(\omega)}, \\
P_{VV}^{(2)}(\omega) &= \frac{z(\omega)[n/m](\omega)}{1 + a_{R,0} z(\omega)} + \frac{z(\omega)[k/l](\omega)}{1 + a_{R,1} z(\omega)} L_s \\
&\quad + s_{VV}^{(2)}(z(w)),
\end{aligned} \tag{9}$$

where $P_{AA-VV}^{(j)}$ is used to approximate the difference between the axial-vector and vector form factors, whereas the vector form factors in isolation are approximated using $P_{VV}^{(j)}$. The limit $z \to \infty$ corresponds to $\omega \to -1$ where the approximants in Eq. (8) approach a constant value. Thus, the rescaling equation (9) enforces the correct asymptotic

[4] To make the double-triangle contribution, shown in Fig. 1, anomaly free, we have to consider doublets of quarks and not just a single (top) quark, but we omit this technicality here since the double-triangle contribution is known and not considered below.

behavior for $z \to \infty$ discussed in Sec. II B and provides us with free parameters $a_{R,i}$ that can be varied in addition to the polynomial degrees n, m, k, and l to assess the stability of the approximation. We note that these variations are performed independently for all the terms in Eq. (9). Our final ansätze for the form factor approximation are then

$$|\tilde{F}^{(j)}_{AA}(z(\omega))\rangle \simeq P^{(j)}_{AA-VV}(\omega) + P^{(j)}_{VV}(\omega), \tag{10}$$

$$|\tilde{F}^{(j)}_{VV}(z(\omega))\rangle \simeq P^{(j)}_{VV}(\omega). \tag{11}$$

It should be noted that our ansatz does not account for and cannot reproduce the aforementioned t- and u-channel branch cuts in the unphysical region $\omega < 0$. Even in the physical region not much is known from first principles concerning the convergence behavior of Padé approximation. In the absence of exact results, our approximation could be compared to, we therefore rely on heuristic arguments.

The approximation method used in this work was shown to reliably reproduce the exact NLO correction for the very similar scenario of di-Higgs production [28]. The main difference is the structure of the couplings to the produced bosons in the considered box diagrams. However, as will be shown in Sec. IV, this difference appears to have no visible impact when applying the method at LO and the convergence behavior at NLO indeed turns out to be similar to the case of di-Higgs production. We find that including more input terms in the construction of the approximation stabilizes the prediction and reduces the estimated uncertainty.

IV. RESULTS

Before showing our results at NLO for the form factors, we can compare the LO form factors constructed as discussed in the previous sections with the full analytic result. We choose as input for the on-shell Z-boson and top quark masses

$$m_Z = 91.1876 \text{ GeV}, \qquad m_t = 173 \text{ GeV} \tag{12}$$

and show results for two different values of $\tilde{x}$ in Fig. 2. The plots contain the maximum information we have available from the LME at LO (see [27]) and our threshold

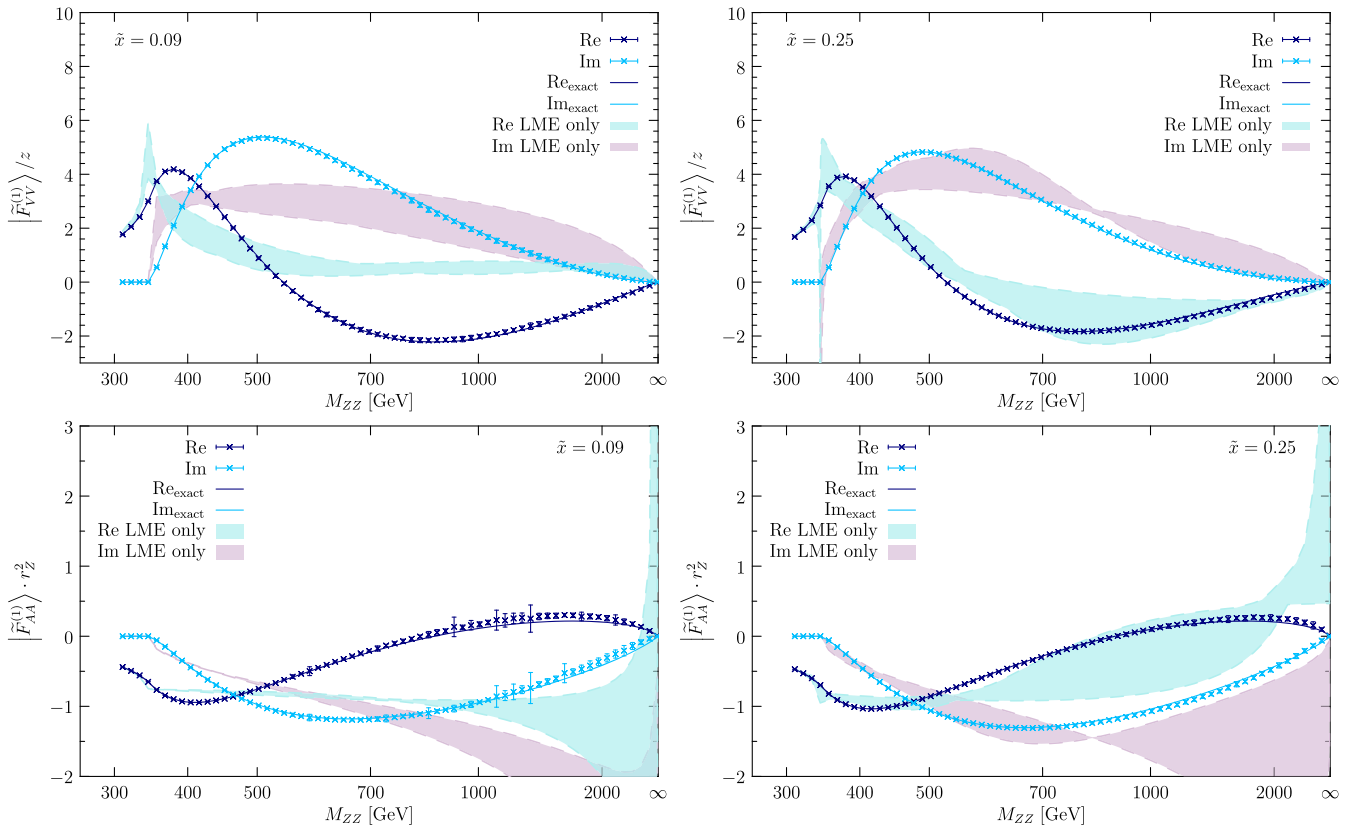

FIG. 2. The form factors $|\tilde{F}^{(1)}_{VV}\rangle$ (upper row) and $|\tilde{F}^{(1)}_{AA}\rangle$ (lower row) at LO for $\tilde{x} = 0.09$ (left side) and $\tilde{x} = 0.25$ (right side) as a function of the invariant mass of the Z-boson pair. $\tilde{x} = 0.25$ corresponds to the maximum possible transverse momentum for a given invariant mass. The dark blue and light blue points correspond to the real and imaginary parts of the Padé approximants from Eqs. (10) and (11); the solid lines are the full result and the shaded regions are Padé approximants that were constructed using only the information from the LME (cf. text for details).

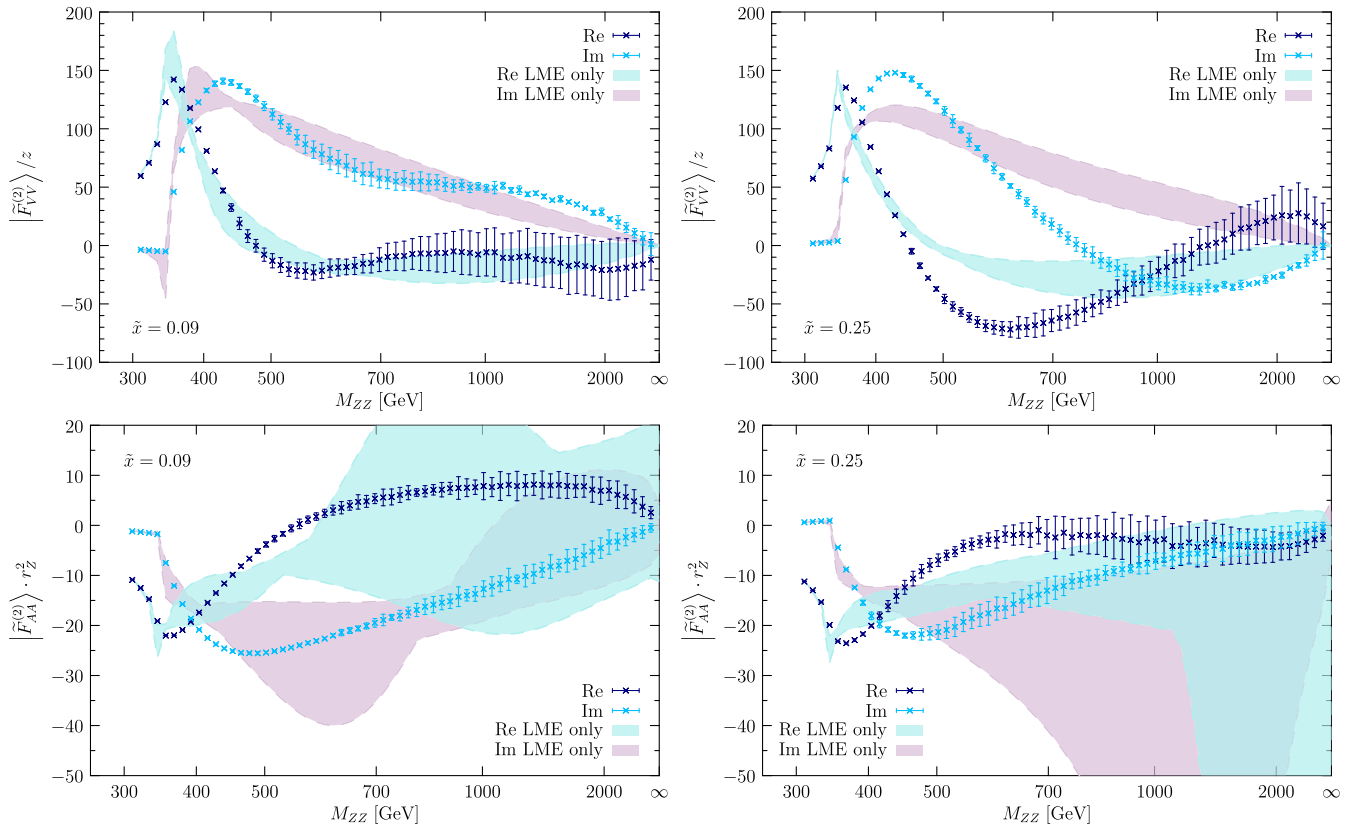

FIG. 3. The NLO form factors $|\tilde{F}^{(2)}_{VV}\rangle$ (upper row) and $|\tilde{F}^{(2)}_{AA}\rangle$ (lower row) for $\tilde{x} = 0.09$ (left side) and $\tilde{x} = 0.25$ (right side) as a function of the invariant mass of the Z-boson pair. The conventions are the same as in Fig. 2 with the points and shaded regions corresponding to the Padé approximation constructed from the LME only.

expansion. By construction the Padé ansatz in Eq. (8) may contain poles anywhere in the complex ω plane whereas the functions it approximates are analytic apart from the branch cuts discussed in Sec. III.[5] Since we aim to reconstruct the form factors in the timelike region, we exclude approximants that exhibit poles for

$$\mathrm{Re}(z(\omega)) > 0 \quad \text{and} \quad |\omega| < 1.2. \tag{13}$$

We obtain an uncertainty estimate for our results in the following way. For every phase space point, we calculate the mean and standard deviation for each contributing Padé approximant in Eq. (9). To this end, we vary the rescaling parameters $a_{R,i}$ in the region

$$a_{R,i} \in [0.1, 10] \tag{14}$$

and vary $[n/m]$ within $|n - m| \leq 3$, where $n + m + 1$ is the number of available constraints. We construct 100 variants for each Padé approximant. Our final prediction then follows from the sum of the mean values of the Padé approximants, with an uncertainty obtained by adding the individual errors in quadrature.

Figure 2 shows the Padé approximants from Eqs. (10) and (11) for the LO form factors $|\tilde{F}^{(1)}_{VV}\rangle$ and $|\tilde{F}^{(1)}_{AA}\rangle$ including our uncertainty estimate as points with error bars. We observe good agreement with the full results, which are indicated by the solid lines, up to large values of the invariant mass M_{ZZ} of the Z-boson pair. The error remains small throughout the whole invariant mass range, increasing somewhat toward large M_{ZZ}. The behavior for different values of $\tilde{x}$ is similar. To demonstrate the importance of including the threshold expansion, we also show an approximation based solely on the LME as shaded regions. For this, we adopt the prescription given in Ref. [27] and show the envelope of the [2/2], [2/3], [3/2], and [3/3] Padé approximants which we have constructed without applying the rescaling of Eq. (9) or the pole criterion Eq. (13). We note that the resonant structure near $z = 1$ in the upper right plot showing the vector form factor for maximal transverse momentum is caused by a pole near $w = 1$ in the [3/3] Padé approximant. In our full results, from Eqs. (10) and (11), we apply the criterion Eq. (13) to exclude approximants which feature such resonances in the timelike region $z \geq 0$.

[5]For the case of the more well-behaved heavy-quark vacuum polarization, it was found that the poles in the Padé approximants mimic the physical branch cut [52].

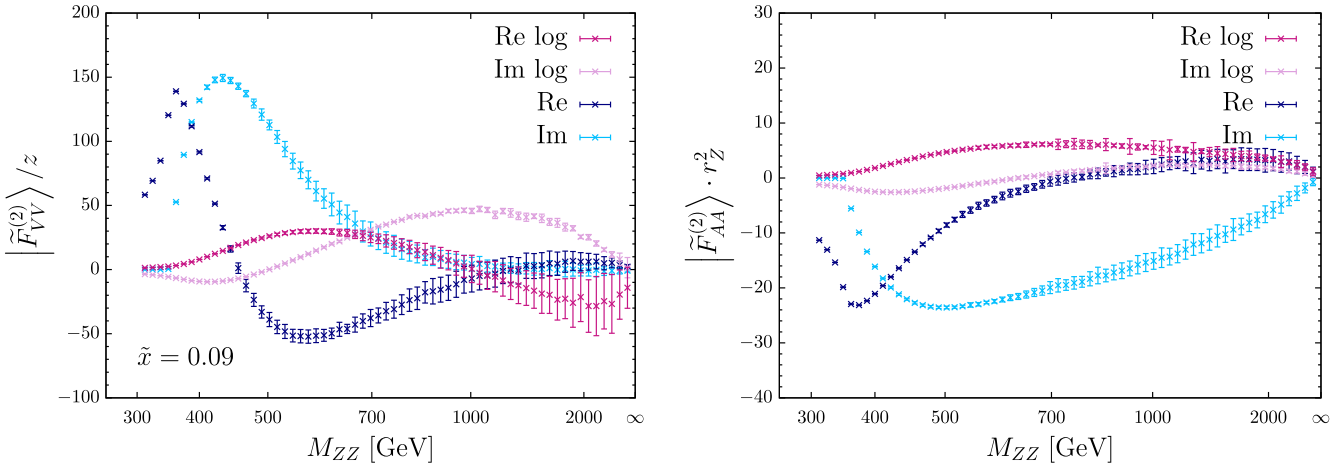

FIG. 4. Logarithmic (log) and nonlogarithmic contributions to the vector and axial-vector form factors.

We conclude that the threshold expansion is essential for the reconstruction of the full top mass dependence above the top quark threshold.

We now turn to the NLO form factors. In Fig. 3, we show the results for the virtual corrections to the form factors $|\tilde{F}^{(2)}_{VV}\rangle$ (upper panel) and $|\tilde{F}^{(2)}_{AA}\rangle$ (lower panel) for two values of $\tilde{x}$. Note that we do not include the double-triangle contribution to the form factors, as they have been computed analytically in [27]. As at LO, we include only the top quark contributions. The uncertainty associated with the Padé construction increases with M_{ZZ}. Since we input information mainly at low M_{ZZ}, this behavior is expected. With the exception of the vector form factor $|\tilde{F}^{(2)}_{VV}\rangle$ for small transverse momenta (upper left panel in Fig. 3), we find that the Padé approximation based on the LME alone does not yield a realistic reconstruction of the top-quark mass effects of the form factors. In particular, the important axial-vector form factor suffers from very large uncertainties. We remark though that in [27] for the NLO cross section the Padé prediction was improved by a reweighting with the full LO cross section.

We note that $|\tilde{F}^{(2)}_{VV}\rangle$ shows a small oscillation in the region of large M_{ZZ} when the transverse momentum of the Z bosons is small as is evident from the upper left plot in Fig. 3. We trace the appearance of the second peak back to the contribution proportional to L_s stemming from diagrams with massless cuts. As shown in Fig. 4, this logarithmic contribution is numerically important in the vector form factor for large M_{ZZ} but significantly smaller than the nonlogarithmic contribution in the axial-vector form factor. In general, we find that the contribution proportional to L_s shows worse convergence behavior than the nonlogarithmic terms when including more and more terms in the LME and the threshold expansion. This is shown in Fig. 5 where we compare our results from Fig. 3 to the Padé approximants obtained with the same procedure but only using threshold input up to the order $\bar{z}^2$ and $\bar{z}^3$. We observe good convergence in the case of the axial-vector form factor. On the other hand, the $\mathcal{O}(\bar{z}^2)$ approximation for the vector form factor does not feature the oscillatory behavior described above and there is no overlap with the full approximation in a significant part of the phase space. However, the $\mathcal{O}(\bar{z}^3)$ and $\mathcal{O}(\bar{z}^4)$ results are in good agreement with the full approximation where we have also included the $\mathcal{O}(\bar{z}^5)$ term in the coefficient of the logarithm L_s to verify that this stabilization persists with the addition of higher orders in the threshold expansion. We conclude from this discussion, that the Padé approximation can be improved systematically when including higher orders in the various expansions. Nevertheless, we believe that the prediction for $|\tilde{F}^{(2)}_{VV}\rangle$ should be taken with a grain of salt above $M_{ZZ} \geq 500$ GeV because of the slower convergence. We note also that we find very similar convergence behavior as in the case of Higgs boson pair production, discussed in [28]. As we found here for ZZ, the contributions from diagrams proportional to L_s and hence massless cuts converge worse than the nonlogarithmic pieces.

In Fig. 6, we show the virtual corrections to the form factor $v_f^2|\tilde{F}^{(2)}_{VV}\rangle + a_f^2|\tilde{F}^{(2)}_{AA}\rangle$ as it enters in the interference term with the Higgs boson exchange. We expect a large suppression of the vector contribution since $v_f^2 \ll a_f^2$ and the LME of the vector form factor only starts one order higher [27]. Indeed, we find that $v_f^2|\tilde{F}^{(2)}_{VV}\rangle$ has to be amplified by a factor of 300 to be comparable to the axial-vector contribution, cf. the dashed lines in Fig. 6. This clearly demonstrates that the interference term will be dominated by $|\tilde{F}^{(2)}_{AA}\rangle$, and we therefore choose not to modify the uncertainty estimate for the vector form factor. The fact that $|\tilde{F}^{(2)}_{VV}\rangle$ is negligible compared to $|\tilde{F}^{(2)}_{AA}\rangle$ allows us to make trustworthy predictions for the interference with the Higgs production with subsequent decay to Z bosons up to

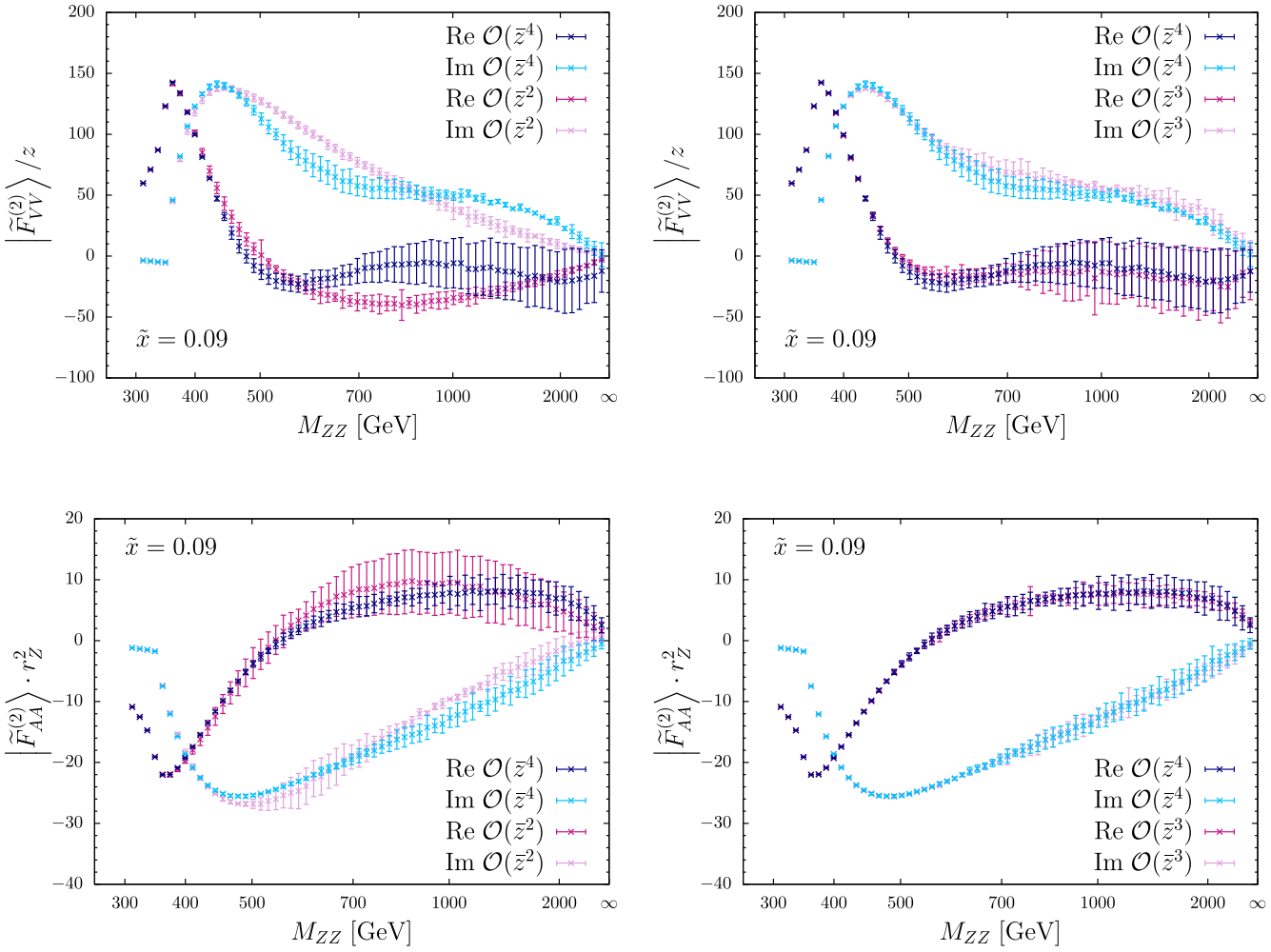

FIG. 5. The NLO form factors $|\tilde{F}^{(2)}_{VV}\rangle$ (upper row) and $|\tilde{F}^{(2)}_{AA}\rangle$ (lower row) for $\tilde{x} = 0.09$ as a function of the invariant mass of the Z-boson pair. In dark/light blue, we show the same points as in Fig. 3 while in pink/rose we show the real/imaginary part of the Padé approximants expanded up to $\mathcal{O}(\bar{z}^2)$ (left side) and $\mathcal{O}(\bar{z}^3)$ (right side).

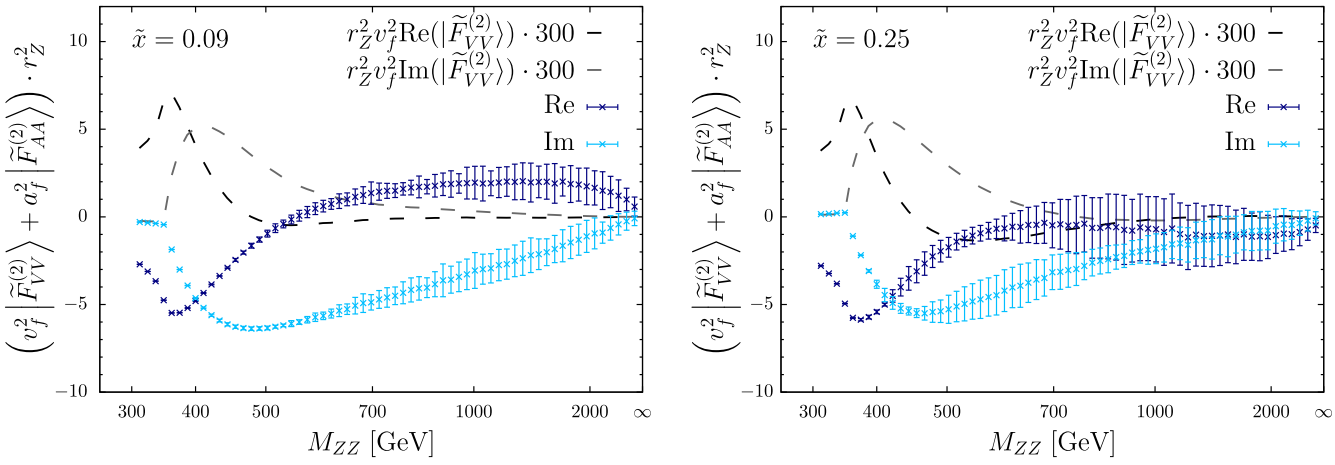

FIG. 6. The interference form factor $v_f^2|\tilde{F}^{(2)}_{VV}\rangle + a_f^2|\tilde{F}^{(2)}_{VV}\rangle$ for $\tilde{x} = 0.09$ (left side) and $\tilde{x} = 0.25$ (right side) as a function of the invariant mass of the Z-boson pair. The dashed lines show a rescaled form factor $|\tilde{F}^{(2)}_{VV}\rangle$ to demonstrate that it is negligible compared to $|\tilde{F}^{(2)}_{AA}\rangle$.

$M_{ZZ} \to \infty$, even though as stated above we trust our results for $|\tilde{F}_{VV}^{(2)}\rangle$ only for $M_{ZZ} \leq 500$ GeV.

The numerical implementation of the form factors is available as a FORTRAN routine on request and can be combined with existing computations of the massless loop contributions and the real corrections for the interference of the Higgs exchange with decay to ZZ with the continuum background.

V. CONCLUSIONS AND OUTLOOK

We have considered top-quark mass effects in the continuum process $gg \to ZZ$, focusing on the form factors relevant for the NLO interference with the production of a Higgs boson and its subsequent decay into two Z bosons. We have presented a Padé-based approximation using information from an expansion around a large top quark mass and an expansion around the top quark pair production threshold.

At LO, we have shown that our Padé construction approximates very well the full top mass dependence of the form factors for the whole range of the invariant mass M_{ZZ} of the Z bosons. At NLO, we provide a new prediction with very small uncertainties at small and moderate M_{ZZ}, with an increased uncertainty toward large M_{ZZ}. We expect that adding more information into the Padé construction at large M_{ZZ} would improve the description also in this region.

Our results can be combined both with virtual corrections mediated by massless loops and the real corrections. The latter constitute a one-loop process and can therefore be computed with well-established techniques. The Padé construction can also be applied to the remaining form factors contributing to $gg \to ZZ$, which do not interfere with the Higgs signal.

We note also that while in this work we have applied our method to the production of on-shell Z bosons, there is no obstruction for applying it also to off-shell Z-boson production. Indeed, the LME for off-shell Z-boson production is already known up to the order z^4 [24]. While a calculation of the full top mass dependence for on-shell Z bosons with numerical methods seems to be feasible with current techniques in a reasonable timeframe (see [53,54]), a computation of the off-shell form factors appears to be beyond the current state-of-the-art.

ACKNOWLEDGMENTS

We thank B. Agarwal, A. von Manteuffel, and N. Kauer for their comments on the manuscript. This work has received funding from the European Union's Horizon 2020 research and innovation programme under the Marie Skłodowska-Curie grant Agreement No. 764850, SAGEX. R. G. is supported by the "Berliner Chancengleichheitsprogramm."

APPENDIX A: THRESHOLD EXPANSION OF FORM FACTORS

In the following, we give explicit expressions for the coefficients in the threshold expansions of the form factors. For convenience, we quote the definition already given in Eq. (5),

$$|\tilde{\mathcal{F}}_i^{(1)}\rangle \overset{z\to 1}{\asymp} \sum_{n=3}^{\infty} a_i^{(n,0)} \bar{z}^{\frac{n}{2}}, \tag{A1}$$

$$|\tilde{\mathcal{F}}_i^{(2)}\rangle \overset{z\to 1}{\asymp} \sum_{n=2}^{\infty} \sum_{m=\bar{n}_2}^{1} [b_i^{(n,m)} + b_{i,\ln}^{(n,m)} \ln(-4z)] \bar{z}^{\frac{n}{2}} \ln^m \bar{z}, \tag{A2}$$

where $i \in \{VV, AA\}$ and $\bar{n}_2$ is n modulo 2. The coefficients a, b are most conveniently written in terms of the two dimensionless ratios $r_Z = \frac{m_Z^2}{M_{ZZ}^2}$ and $r_{p_T} = \frac{p_T^2}{M_{ZZ}^2} = \tilde{x} - r_Z$. We define the loop integral measure as

$$[dl] = \frac{d^d l}{i\pi^{\frac{d}{2}}} e^{\epsilon\gamma_E} \tag{A3}$$

and use the shorthand notation

$$C_0 = \int [dl] \frac{1}{l^2[(l+q)^2 - 1][(l+q-p_Z)^2 - 1]}, \tag{A4}$$

with $q^2 = 1, p_Z^2 = 4r_Z^2, q \cdot p_Z = 1$. The coefficients $b_{i,\ln}^{(n,1)}$ and $b_{i,\ln}^{(2n,m)}$ vanish. Furthermore, coefficients with $m = 0$ and even n do not contribute to the imaginary part and are therefore not listed here. We have calculated the remaining coefficients $a_i^{n,0}, b_i^{n,m}$ up to $n = 8$ and the coefficients $b_{i,\ln}^{(n,0)}$ up to $n = 9$, obtaining the following results:

$$a_{AA}^{(3,0)} = \frac{4\pi}{3(1-2r_Z)^2 r_Z^2}(-1 + 6r_Z - 18r_Z^2 + 16r_Z^3), \tag{A5}$$

$$a_{AA}^{(5,0)} = \frac{2\pi}{15(1-2r_Z)^4 r_Z^2}[-21 + 210r_Z - 958r_Z^2 + 2336r_Z^3 - 2968r_Z^4 + 1472r_Z^5 + 8r_{p_T}(1-2r_Z)^2(1-2r_Z+4r_Z^2)], \tag{A6}$$

$$\begin{aligned} a_{AA}^{(7,0)} = \frac{\pi}{210(1-2r_Z)^6 r_Z^2}[&-905 + 12670r_Z - 80954r_Z^2 + 301104r_Z^3 - 695264r_Z^4 + 985120r_Z^5 \\ &- 788896r_Z^6 + 269568r_Z^7 + 16r_{p_T}(1-2r_Z)^2(39 - 234r_Z + 672r_Z^2 - 920r_Z^3 + 592r_Z^4)], \end{aligned} \tag{A7}$$

$$b_{AA}^{(2,1)} = \frac{32\pi^2}{9(1-2r_Z)^2 r_Z^2}(-1+6r_Z-18r_Z^2+16r_Z^3), \tag{A8}$$

$$\begin{aligned} b_{AA}^{(3,0)} = &-\frac{\pi}{9(1-2r_Z)^3(1-4r_Z)^2 r_Z^2}[-2(1-2r_Z)(1-4r_Z)^2[-136+3\pi^2+168\ln(2)]r_{p_T}(1-2r_Z+4r_Z^2) \\ &- 64C_0(1-2r_Z)^2(1-4r_Z)^2(-1-7r_Z+34r_Z^2-44r_Z^3+8r_Z^4) \\ &+ 64r_Z(1-4r_Z)^2\sqrt{\frac{1-r_Z}{r_Z}}\arctan\left(\frac{2\sqrt{(1-r_Z)r_Z}}{1-2r_Z}\right)(9-45r_Z+70r_Z^2-56r_Z^3+32r_Z^4) \\ &- (1-2r_Z)(1-4r_Z)[192+9\pi^2-56\ln(2)-1728r_Z-90\pi^2 r_Z+560\ln(2)r_Z+6256r_Z^2+384\pi^2 r_Z^2 \\ &\quad - 2016\ln(2)r_Z^2-12480r_Z^3-816\pi^2 r_Z^3+3584\ln(2)r_Z^3+12032r_Z^4+576\pi^2 r_Z^4-3584\ln(2)r_Z^4-2048r_Z^5] \\ &+ 128(1-2r_Z)\ln(2-4r_Z)(2-23r_Z+98r_Z^2-184r_Z^3+152r_Z^4-112r_Z^5+96r_Z^6)], \end{aligned} \tag{A9}$$

$$b_{AA,\ln}^{(3,0)} = 0, \tag{A10}$$

$$b_{AA}^{(3,1)} = 0, \tag{A11}$$

$$b_{AA}^{(4,1)} = \frac{32\pi^2}{45(1-2r_Z)^4 r_Z^2}[-3+30r_Z-134r_Z^2+328r_Z^3-464r_Z^4+256r_Z^5+4(1-2r_Z)^2 r_{p_T}(1-2r_Z+4r_Z^2)], \tag{A12}$$

$$\begin{aligned} b_{AA}^{(5,0)} = &\frac{\pi}{4050(1-2r_Z)^5(1-4r_Z)^3 r_Z^2}[-(1-2r_Z)(1-4r_Z)[21472-6075\pi^2-104520\ln(2)-643776r_Z \\ &+ 109350\pi^2 r_Z+1881360\ln(2)r_Z+7528432r_Z^2-855900\pi^2 r_Z^2-14848320\ln(2)r_Z^2-44282176r_Z^3 \\ &+ 3817800\pi^2 r_Z^3+67172160\ln(2)r_Z^3+141881152r_Z^4-10558080\pi^2 r_Z^4-187708800\ln(2)r_Z^4 \\ &- 245787136r_Z^5+18135360\pi^2 r_Z^5+319941120\ln(2)r_Z^5+202149888r_Z^6-17763840\pi^2 r_Z^6 \\ &- 302008320\ln(2)r_Z^6-35688448r_Z^7+7326720\pi^2 r_Z^7+117350400\ln(2)r_Z^7-25067520r_Z^8] \\ &- 18(1-2r_Z)(1-4r_Z)r_{p_T}[2136+375\pi^2-360\ln(2)-37584r_Z-5250\pi^2 r_Z+5040\ln(2)r_Z \\ &+ 263040r_Z^2+30000\pi^2 r_Z^2-28800\ln(2)r_Z^2-915648r_Z^3-94200\pi^2 r_Z^3+22080\ln(2)r_Z^3 \\ &+ 1546624r_Z^4+184560\pi^2 r_Z^4+424320\ln(2)r_Z^4-1103872r_Z^5-218880\pi^2 r_Z^5 \\ &- 1320960\ln(2)r_Z^5+546816r_Z^6+111360\pi^2 r_Z^6+768000\ln(2)r_Z^6-163840r_Z^7] \\ &+ C_0(1-2r_Z)(1-4r_Z)[46080(1-2r_Z)^3 r_{p_T}(2-9r_Z+20r_Z^2-12r_Z^3-8r_Z^4+16r_Z^5) \\ &- 2880(1-2r_Z)(1-4r_Z)(31-99r_Z-1242r_Z^2+8912r_Z^3-23696r_Z^4+29840r_Z^5-16608r_Z^6+2176r_Z^7)] \\ &+ r_Z(1-4r_Z)\sqrt{\frac{1-r_Z}{r_Z}}\arctan\left(\frac{2\sqrt{(1-r_Z)r_Z}}{1-2r_Z}\right)[960(1-4r_Z)(-687+8843r_Z \\ &- 46162r_Z^2+126356r_Z^3-195416r_Z^4+174304r_Z^5-95360r_Z^6+30720r_Z^7) \\ &- 46080(1-2r_Z)^2 r_{p_T}(-6+45r_Z-152r_Z^2+264r_Z^3-176r_Z^4+16r_Z^5)] \\ &+ (1-2r_Z)\ln(2-4r_Z)[1920(-170+3251r_Z-26282r_Z^2+117196r_Z^3-314896r_Z^4 \\ &+ 524464r_Z^5-549440r_Z^6+394688r_Z^7-240512r_Z^8+96768r_Z^9) \\ &- 92160(1-2r_Z)^2 r_{p_T}(-1+13r_Z-70r_Z^2+200r_Z^3-280r_Z^4+128r_Z^5)]], \end{aligned} \tag{A13}$$

$$b_{AA,\ln}^{(5,0)} = \frac{16\pi}{5(1-2r_Z)^2 r_Z^2}(-1+4r_Z+6r_{p_T})(1-2r_Z+4r_Z^2), \tag{A14}$$

$$b_{AA}^{(5,1)} = \frac{32\pi}{135(1-2r_Z)^2 r_Z^2}[53-318r_Z+846r_Z^2-848r_Z^3-108r_{p_T}(1-2r_Z+4r_Z^2)], \tag{A15}$$

$$b_{AA}^{(6,1)} = \frac{32\pi^2}{315(1-2r_Z)^6 r_Z^2}[19 - 266r_Z + 1730r_Z^2 - 6504r_Z^3 + 14648r_Z^4 - 19072r_Z^5 + 12128r_Z^6 - 2816r_Z^7 + 4(1-2r_Z)^2 r_{p_T}(9 - 54r_Z + 168r_Z^2 - 208r_Z^3 + 128r_Z^4)], \tag{A16}$$

$$\begin{aligned} b_{AA}^{(7,0)} = {} & \frac{\pi}{793800(1-r_Z)(1-2r_Z)^7(1-4r_Z)^4 r_Z^2}[(1-r_Z)(1-2r_Z)(1-4r_Z)[-48296976 + 1306935\pi^2 \\ & + 68546520\ln(2) + 1381163616r_Z - 33980310\pi^2 r_Z - 1782209520\ln(2)r_Z - 19953987184r_Z^2 \\ & + 396287640\pi^2 r_Z^2 + 20934631200\ln(2)r_Z^2 + 178890721728r_Z^3 - 2743009920\pi^2 r_Z^3 \\ & - 146825159040\ln(2)r_Z^3 - 1038970811008r_Z^4 + 12546379440\pi^2 r_Z^4 + 682278602880\ln(2)r_Z^4 \\ & + 3951328802304r_Z^5 - 39832823520\pi^2 r_Z^5 - 2194951852800\ln(2)r_Z^5 - 9798614287104r_Z^6 \\ & + 89300171520\pi^2 r_Z^6 + 4941762577920\ln(2)r_Z^6 + 15459576751104r_Z^7 - 140100468480\pi^2 r_Z^7 \\ & - 7665966120960\ln(2)r_Z^7 - 14595082354688r_Z^8 + 147641840640\pi^2 r_Z^8 + 7817008496640\ln(2)r_Z^8 \\ & + 7124726562816r_Z^9 - 94379765760\pi^2 r_Z^9 - 4715940741120\ln(2)r_Z^9 - 1110704586752r_Z^{10} \\ & + 27358248960\pi^2 r_Z^{10} + 1270490726400\ln(2)r_Z^{10} - 100576788480r_Z^{11}] \\ & + 2(1-r_Z)(1-2r_Z)(1-4r_Z)r_{p_T}[12875128 - 2482515\pi^2 - 32397960\ln(2) - 322712656r_Z \\ & + 54615330\pi^2 r_Z + 712755120\ln(2)r_Z + 3481217888r_Z^2 - 530889660\pi^2 r_Z^2 - 7045775520\ln(2)r_Z^2 \\ & - 21890762240r_Z^3 + 3016742400\pi^2 r_Z^3 + 41557608960\ln(2)r_Z^3 + 89967740544r_Z^4 - 11128456080\pi^2 r_Z^4 \\ & - 162222883200\ln(2)r_Z^4 - 251512872192r_Z^5 + 27788412960\pi^2 r_Z^5 + 434414211840\ln(2)r_Z^5 \\ & + 477015472640r_Z^6 - 47130431040\pi^2 r_Z^6 - 795771594240\ln(2)r_Z^6 - 592554727424r_Z^7 \\ & + 52573812480\pi^2 r_Z^7 + 963913574400\ln(2)r_Z^7 + 437616467968r_Z^8 - 35230325760\pi^2 r_Z^8 \\ & - 705638277120\ln(2)r_Z^8 - 137703424000r_Z^9 + 10818662400\pi^2 r_Z^9 + 235343216640\ln(2)r_Z^9 \\ & - 8257536000r_Z^{10}] \\ & + 201600(1-2r_Z)^3(1-4r_Z)^4[-356 + 3\pi^2 + 520\ln(2)]r_{p_T}^2(-1+r_Z)(1-2r_Z+4r_Z^2) \\ & + C_0(1-r_Z)(1-2r_Z)^2(1-4r_Z)^2[-20160(1-4r_Z)(1773 - 13705r_Z - 15494r_Z^2 + 542860r_Z^3 \\ & - 2672760r_Z^4 + 6652528r_Z^5 - 9490464r_Z^6 + 7595840r_Z^7 - 2952064r_Z^8 + 311808r_Z^9) \\ & + 645120(1-2r_Z)^2 r_{p_T}(96 - 601r_Z + 1800r_Z^2 - 4344r_Z^3 + 7592r_Z^4 - 5664r_Z^5 - 32r_Z^6 + 1600r_Z^7)] \\ & + r_Z(1-4r_Z)^2\sqrt{\frac{1-r_Z}{r_Z}}\arctan\left(\frac{2\sqrt{(1-r_Z)r_Z}}{1-2r_Z}\right)[-6720(1-4r_Z)(35337 - 616496r_Z \\ & + 4722401r_Z^2 - 20896358r_Z^3 + 59069448r_Z^4 - 111353552r_Z^5 + 142045200r_Z^6 \\ & - 122427488r_Z^7 + 70734336r_Z^8 - 26438656r_Z^9 + 5122048r_Z^{10}) \\ & - 215040(1-r_Z)(1-2r_Z)^2 r_{p_T}(-1044 + 10253r_Z - 43216r_Z^2 \\ & + 104204r_Z^3 - 158912r_Z^4 + 150832r_Z^5 - 70976r_Z^6 + 9408r_Z^7)] \\ & - \ln(2-4r_Z)(1-r_Z)(1-2r_Z)[13440(9662 - 255657r_Z + 3011806r_Z^2 - 20841376r_Z^3 \\ & + 94139672r_Z^4 - 291779424r_Z^5 + 635459136r_Z^6 - 982191360r_Z^7 + 1084817792r_Z^8 \\ & - 874003712r_Z^9 + 538395136r_Z^{10} - 253452288r_Z^{11} + 66985984r_Z^{12}) \\ & + 430080(1-2r_Z)^2 r_{p_T}(-251 + 4211r_Z - 30950r_Z^2 + 132676r_Z^3 - 370528r_Z^4 \\ & + 699712r_Z^5 - 871904r_Z^6 + 647168r_Z^7 - 220160r_Z^8 + 18432r_Z^9)]], \end{aligned} \tag{A17}$$

$$b_{AA,\ln}^{(7,0)} = \frac{8\pi}{35(1-2r_Z)^4 r_Z^2}(-1+4r_Z+6r_{p_T})(39-234r_Z+672r_Z^2-920r_Z^3+592r_Z^4), \tag{A18}$$

$$\begin{aligned} b_{AA}^{(7,1)} = \frac{16\pi}{945(1-2r_Z)^4 r_Z^2}&[2079-20790r_Z+91822r_Z^2-218096r_Z^3+269368r_Z^4-137024r_Z^5 \\ &-4r_{p_T}(1169-7014r_Z+20000r_Z^2-27624r_Z^3+17840r_Z^4)], \end{aligned} \tag{A19}$$

$$\begin{aligned} b_{AA}^{(8,1)} = \frac{32\pi^2}{945(1-2r_Z)^8 r_Z^2}&[233-4194r_Z+34914r_Z^2-174856r_Z^3+575264r_Z^4 \\ &-1278272r_Z^5+1903168r_Z^6-1816064r_Z^7+992768r_Z^8-235520r_Z^9 \\ &+4(1-2r_Z)^2 r_{p_T}(11-110r_Z+572r_Z^2-1544r_Z^3+2288r_Z^4-1184r_Z^5+192r_Z^6) \\ &-64(1-2r_Z)^4 r_{p_T}^2(1-2r_Z+4r_Z^2)], \end{aligned} \tag{A20}$$

$$\begin{aligned} b_{AA,\ln}^{(9,0)} = \frac{-2\pi}{315(1-2r_Z)^6 r_Z^2}&[2621-36694r_Z+225124r_Z^2-793216r_Z^3+1727344r_Z^4-2317408r_Z^5+1757888r_Z^6 \\ &-610560r_Z^7-2r_{p_T}(8183-81830r_Z+373652r_Z^2-964400r_Z^3+1472912r_Z^4-1224416r_Z^5+457920r_Z^6) \\ &+3200r_{p_T}^2(1-2r_Z)^2(1-2r_Z+4r_Z^2)] \end{aligned} \tag{A21}$$

for the expansion of the axial-vector component. The corresponding coefficients in the expansion of the vector part read

$$a_{VV}^{(3,0)} = \frac{16\pi}{3(1-2r_Z)^2}(2-5r_Z), \tag{A22}$$

$$a_{VV}^{(5,0)} = \frac{8\pi}{15(1-2r_Z)^4}[34-217r_Z+492r_Z^2-412r_Z^3+8(1-2r_Z)^2 r_{p_T}], \tag{A23}$$

$$\begin{aligned} a_{VV}^{(7,0)} = \frac{2\pi}{105(1-2r_Z)^6}&[1314-13549r_Z+57240r_Z^2-124296r_Z^3+141056r_Z^4-70032r_Z^5 \\ &+16(1-2r_Z)^2 r_{p_T}(11-72r_Z+148r_Z^2)], \end{aligned} \tag{A24}$$

$$b_{VV}^{(2,1)} = \frac{128\pi^2}{9(1-2r_Z)^2}(2-5r_Z), \tag{A25}$$

$$\begin{aligned} b_{VV}^{(3,0)} = -\frac{\pi}{9(1-2r_Z)^3(1-4r_Z)^2}&[4(1-2r_Z)(1-4r_Z)(136+21\pi^2+56\ln(2)-680r_Z \\ &-138\pi^2 r_Z-448\ln(2)r_Z+480r_Z^2+216\pi^2 r_Z^2+896\ln(2)r_Z^2+512r_Z^3) \\ &-8(1-2r_Z)(1-4r_Z)^2(-136+3\pi^2+168\ln(2))r_{p_T} \\ &-128C_0(1-2r_Z)^2(1-4r_Z)^2(-3+4r_Z^2) \\ &+64(1-4r_Z)^2\sqrt{\frac{1-r_Z}{r_Z}}\arctan\left(\frac{2\sqrt{(1-r_Z)r_Z}}{1-2r_Z}\right)(-5+46r_Z-96r_Z^2+32r_Z^3) \\ &+512(1-2r_Z)\ln(2-4r_Z)(2-23r_Z+86r_Z^2-112r_Z^3+24r_Z^4)], \end{aligned} \tag{A26}$$

$$b_{VV,\ln}^{(3,0)} = 0, \tag{A27}$$

$$b_{VV}^{(3,1)} = 0, \tag{A28}$$

$$b_{VV}^{(4,1)} = \frac{128\pi^2}{45(1-2r_Z)^4}(2-11r_Z+36r_Z^2-56r_Z^3+4(1-2r_Z)^2 r_{p_T}), \tag{A29}$$

$$
\begin{aligned}
b_{VV}^{(5,0)} = &-\frac{\pi}{2025(1-r_Z)(1-2r_Z)^5(1-4r_Z)^3}[-2(1-2r_Z)(1-4r_Z)(1-r_Z)(186008-6345\pi^2-177000\ln(2)\\
&-2712968r_Z+88830\pi^2 r_Z+2535360\ln(2)r_Z+15732800r_Z^2-498420\pi^2 r_Z^2-14241120\ln(2)r_Z^2\\
&-45725792r_Z^3+1443960\pi^2 r_Z^3+39511680\ln(2)r_Z^3+68432384r_Z^4-2246400\pi^2 r_Z^4\\
&-55011840\ln(2)r_Z^4-45982208r_Z^5+1537920\pi^2 r_Z^5+31488000\ln(2)r_Z^5+6266880r_Z^6)\\
&+36(1-2r_Z)(1-4r_Z)(1-r_Z)r_{p_T}(-8024+585\pi^2+11400\ln(2)+97248r_Z-6900\pi^2 r_Z\\
&-130080\ln(2)r_Z-384928r_Z^2+28860\pi^2 r_Z^2+505440\ln(2)r_Z^2+532224r_Z^3-49440\pi^2 r_Z^3\\
&-718080\ln(2)r_Z^3-88576r_Z^4+27840\pi^2 r_Z^4+192000\ln(2)r_Z^4-40960r_Z^5)\\
&+C_0(1-r_Z)(1-2r_Z)^2(1-4r_Z)[2880(1-4r_Z)(53-564r_Z+2000r_Z^2-2368r_Z^3-336r_Z^4+1088r_Z^5)\\
&-46080(1-2r_Z)^2 r_{p_T}(3-24r_Z+40r_Z^2+8r_Z^3)]\\
&+(1-r_Z)(1-2r_Z)\ln(2-4r_Z)[-3840(-80+1549r_Z-12538r_Z^2\\
&+54340r_Z^3-134752r_Z^4+187264r_Z^5-126752r_Z^6+24192r_Z^7)\\
&-92160(1-2r_Z)^2 r_{p_T}(-1+16r_Z-64r_Z^2+80r_Z^3)]\\
&+\sqrt{\frac{1-r_Z}{r_Z}}\arctan\left(\frac{2\sqrt{(1-r_Z)r_Z}}{1-2r_Z}\right)[480(1-4r_Z)^2(-318+4749r_Z-29882r_Z^2\\
&+103460r_Z^3-212040r_Z^4+249152r_Z^5-144896r_Z^6+30720r_Z^7)\\
&+23040(1-2r_Z)^2(1-4r_Z)(1-r_Z)r_{p_T}(-5+54r_Z-184r_Z^2+200r_Z^3+16r_Z^4)]],
\end{aligned}
\tag{A30}
$$

$$
b_{VV,\ln}^{(5,0)} = \frac{64\pi}{5(1-2r_Z)^2}(-1+4r_Z+6r_{p_T}),
\tag{A31}
$$

$$
b_{VV}^{(5,1)} = \frac{128\pi}{135(1-2r_Z)^2}(-52+103r_Z-108r_{p_T}),
\tag{A32}
$$

$$
b_{VV}^{(6,1)} = \frac{128\pi^2}{315(1-2r_Z)^6}[-58+619r_Z-2624r_Z^2+5540r_Z^3-5552r_Z^4+1648r_Z^5+4(1-2r_Z)^2 r_{p_T}(-5+6r_Z+32r_Z^2)],
\tag{A33}
$$

$$
\begin{aligned}
b_{VV}^{(7,0)} = &-\frac{\pi}{198450(1-2r_Z)^7(1-4r_Z)^4(1-r_Z)^2}[-(1-2r_Z)(1-4r_Z)(1-r_Z)[122096632-127575\pi^2\\
&-92998920\ln(2)-2848934592r_Z+1630125\pi^2 r_Z+2155938120\ln(2)r_Z+29029779592r_Z^2\\
&-2152710\pi^2 r_Z^2-21749266560\ln(2)r_Z^2-169738450784r_Z^3-74541600\pi^2 r_Z^3\\
&+125261747520\ln(2)r_Z^3+628426159680r_Z^4+590919840\pi^2 r_Z^4-453823735680\ln(2)r_Z^4\\
&-1530688965120r_Z^5-2089568880\pi^2 r_Z^5+1072845164160\ln(2)r_Z^5+2460756033152r_Z^6\\
&+3889861920\pi^2 r_Z^6-1656277002240\ln(2)r_Z^6-2533430536704r_Z^7-3445787520\pi^2 r_Z^7\\
&+1613260615680\ln(2)r_Z^7+1538421684224r_Z^8+694310400\pi^2 r_Z^8-902101401600\ln(2)r_Z^8\\
&-445393100800r_Z^9+435456000\pi^2 r_Z^9+220520939520\ln(2)r_Z^9+25144197120r_Z^{10}]\\
&-2(1-2r_Z)(1-4r_Z)(1-r_Z)^2 r_{p_T}[8486296-785295\pi^2-11199720\ln(2)-222273632r_Z\\
&+17777340\pi^2 r_Z+267660960\ln(2)r_Z+2469324096r_Z^2-173313000\pi^2 r_Z^2-2810969280\ln(2)r_Z^2\\
&-14926447104r_Z^3+941371200\pi^2 r_Z^3+16619420160\ln(2)r_Z^3+52801418112r_Z^4-3062631600\pi^2 r_Z^4\\
&-58795390080\ln(2)r_Z^4-108303542784r_Z^5+5922262080\pi^2 r_Z^5+122121377280\ln(2)r_Z^5
\end{aligned}
$$

$$
\begin{aligned}
&+ 116805871616 r_Z^6 - 6230165760\pi^2 r_Z^6 - 134713743360 \ln(2) r_Z^6 - 48174653440 r_Z^7 \\
&+ 2704665600\pi^2 r_Z^7 + 58835804160 \ln(2) r_Z^7 - 2064384000 r_Z^8] \\
&+ 201600(1-2r_Z)^3(1-4r_Z)^4(1-r_Z)^2[-356 + 3\pi^2 + 520\ln(2)] r_{p_T}^2 \\
&+ C_0(1-r_Z)^2(1-2r_Z)^2(1-4r_Z)^2[10080(1-4r_Z)(1879 - 29708 r_Z + 186948 r_Z^2 \\
&- 592848 r_Z^3 + 968208 r_Z^4 - 663104 r_Z^5 - 57920 r_Z^6 + 155904 r_Z^7) \\
&- 322560(1-2r_Z)^2 r_{p_T}(85 - 896 r_Z + 3708 r_Z^2 - 7176 r_Z^3 + 5312 r_Z^4 + 800 r_Z^5)] \\
&+ (1-4r_Z)^2 \sqrt{\frac{1-r_Z}{r_Z}} \arctan\left(\frac{2\sqrt{(1-r_Z)r_Z}}{1-2r_Z}\right)[-1680(1-4r_Z)(14088 - 262050 r_Z \\
&+ 2162807 r_Z^2 - 10516934 r_Z^3 + 33617664 r_Z^4 - 74234384 r_Z^5 + 114844848 r_Z^6 \\
&- 121868128 r_Z^7 + 82948992 r_Z^8 - 31822336 r_Z^9 + 5122048 r_Z^{10}) \\
&- 53760(1-r_Z)(1-2r_Z)^2 r_{p_T}(504 - 7341 r_Z + 44374 r_Z^2 - 142180 r_Z^3 \\
&+ 253056 r_Z^4 - 229360 r_Z^5 + 68704 r_Z^6 + 9408 r_Z^7)] \\
&+ \ln(2-4r_Z)(1-r_Z)^2(1-2r_Z)[13440(2522 - 68893 r_Z + 832786 r_Z^2 - 5869624 r_Z^3 + 26678552 r_Z^4 \\
&- 81564240 r_Z^5 + 169456096 r_Z^6 - 235064576 r_Z^7 + 205653632 r_Z^8 - 98444288 r_Z^9 + 16746496 r_Z^{10}) \\
&+ 215040(1-2r_Z)^2 r_{p_T}(17 - 772 r_Z + 9460 r_Z^2 - 51664 r_Z^3 \\
&+ 146272 r_Z^4 - 212992 r_Z^5 + 124160 r_Z^6 + 9216 r_Z^7)]], \qquad \text{(A34)}
\end{aligned}
$$

$$
b_{VV,\ln}^{(7,0)} = \frac{32\pi}{35(1-2r_Z)^4}(-1 + 4r_Z + 6r_{p_T})(11 - 72 r_Z + 148 r_Z^2), \qquad \text{(A35)}
$$

$$
b_{VV}^{(7,1)} = \frac{64\pi}{945(1-2r_Z)^4}[-2128 + 12817 r_Z - 25428 r_Z^2 + 16060 r_Z^3 + 4 r_{p_T}(-413 + 2408 r_Z - 4460 r_Z^2)], \qquad \text{(A36)}
$$

$$
\begin{aligned}
b_{VV}^{(8,1)} = &\frac{128\pi^2}{945(1-2r_Z)^8}[-430 + 6217 r_Z - 38796 r_Z^2 + 135616 r_Z^3 - 286976 r_Z^4 + 367712 r_Z^5 - 261632 r_Z^6 + 74752 r_Z^7 \\
&+ 4 r_{p_T}(1-2r_Z)^2(-43 + 290 r_Z - 764 r_Z^2 + 808 r_Z^3 + 48 r_Z^4) - 64 r_{p_T}^2(1-2r_Z)^4], \qquad \text{(A37)}
\end{aligned}
$$

$$
\begin{aligned}
b_{VV,\ln}^{(9,0)} = &\frac{8\pi}{315(1-2r_Z)^6}[187 + 564 r_Z - 19112 r_Z^2 + 92640 r_Z^3 - 186896 r_Z^4 + 152640 r_Z^5 \\
&+ r_{p_T}(-482 - 12992 r_Z + 95984 r_Z^2 - 233344 r_Z^3 + 228960 r_Z^4) - 3200(1-2r_Z)^2 r_{p_T}^2]. \qquad \text{(A38)}
\end{aligned}
$$

APPENDIX B: SUBTRACTIONS

In this Appendix, we give the functions s_i with $i \in \{VV, AA\}$ used to subtract the threshold logarithms. We write them in terms of auxiliary subtraction functions s_n, $n \in \mathbb{N}$, i.e.,

$$
s_i^{(2)}(z) = \sum_{n=2}^{\infty} C_{i,n} s_n(z), \qquad \text{(B1)}
$$

where the coefficients $C_{i,n}$ are constants and $s_n \overset{z\to 1}{\asymp} \bar{z}^{\frac{n}{2}} \ln(\bar{z}) + \mathcal{O}(\bar{z}^{\frac{n+1}{2}})$ in the threshold region. We construct these auxiliary functions based on the known analytical results for the vacuum polarization function. The subtraction functions and their threshold expansions are

$$s_2(z) = -\frac{16(1-z)\Pi^{(1),v}(z)}{3z}$$
$$\overset{z\to 1}{\asymp}(1-z)\ln(1-z) - \frac{8}{\pi}(1-z)^{3/2} + \frac{1}{3}(1-z)^2\ln(1-z) - \frac{8}{9\pi}(-5+18\ln(2))(1-z)^{5/2}$$
$$-\frac{16}{3\pi}(1-z)^{5/2}\ln(1-z) - \frac{2}{3}(1-z)^3\ln(1-z) + \frac{1}{675\pi}(14653-26280\ln(2))(1-z)^{7/2}$$
$$-\frac{548}{45\pi}(1-z)^{7/2}\ln(1-z) - 2(1-z)^4\ln(1-z) + \mathcal{O}((1-z)^{9/2}), \tag{B2}$$

$$s_4(z) = -\frac{8}{81\pi^2}\frac{54\pi^2(1-z)^2\Pi^{(1),v}(z) - 41z}{z^2}$$
$$\overset{z\to 1}{\asymp}(1-z)^2\ln(1-z) - \frac{8}{\pi}(1-z)^{5/2} + \frac{4}{3}(1-z)^3\ln(1-z) - \frac{16}{9\pi}(2+\ln(512))(1-z)^{7/2}$$
$$-\frac{16}{3\pi}(1-z)^{7/2}\ln(1-z) + \frac{2}{3}(1-z)^4\ln(1-z) + \mathcal{O}((1-z)^{9/2}), \tag{B3}$$

$$s_5(z) = -\frac{32(1-z)^3G(z)\Pi^{(1),v}(z)}{3\pi z^2} + \frac{656}{81\pi^3 z}$$
$$\overset{z\to 1}{\asymp}\left[-\frac{11}{8} + \ln(8) + \frac{3}{2\pi^2}(-2+7\zeta_3)\right](1-z)^{5/2} + (1-z)^{5/2}\ln(1-z)$$
$$-\frac{2}{\pi}(1-z)^3\ln(1-z) + \frac{1}{48}\left(-145 + 264\ln(2). + \frac{376+924\zeta_3}{\pi^2}\right)(1-z)^{7/2} + \frac{11}{6}(1-z)^{7/2}\ln(1-z)$$
$$-\frac{28}{3\pi}(1-z)^4\ln(1-z) + \mathcal{O}((1-z)^{9/2}), \tag{B4}$$

$$s_6(z) = -\frac{16(1-z)^3\Pi^{(1),v}(z)}{3z^3} + \frac{328}{81\pi^2 z^2} - \frac{6404}{675\pi^2 z}$$
$$\overset{z\to 1}{\asymp}(1-z)^3\ln(1-z) - \frac{8}{\pi}(1-z)^{7/2} + \frac{7}{3}(1-z)^4\ln(1-z) + \mathcal{O}((1-z)^{9/2}), \tag{B5}$$

$$s_7(z) = -\frac{32(1-z)^4G(z)\Pi^{(1),v}(z)}{3\pi z^3} + \frac{656}{81\pi^3 z^2} - \frac{131672}{6075\pi^3 z}$$
$$\overset{z\to 1}{\asymp}\left[-\frac{11}{8} + \ln(8) + \frac{3}{2\pi^2}(-2+7\zeta_3)\right](1-z)^{7/2} + (1-z)^{7/2}\ln(1-z) - \frac{2}{\pi}(1-z)^4\ln(1-z) + \mathcal{O}((1-z)^{9/2}), \tag{B6}$$

$$s_8(z) = -\frac{16(1-z)^4\Pi^{(1),v}(z)}{3z^4} + \frac{328}{81\pi^2 z^3} - \frac{27412}{2025\pi^2 z^2} + \frac{7773424}{496125\pi^2 z}$$
$$\overset{z\to 1}{\asymp}(1-z)^4\ln(1-z) + \mathcal{O}((1-z)^{9/2}), \tag{B7}$$

where we have used the symbol $\asymp$ to denote that terms analytical in $(1-z)$ have been dropped on the right-hand side, and we only use subtractions for the logarithmic terms, hence no subtraction functions $s_1(z)$ and $s_3(z)$ are necessary. We have used

$$G(z) = \frac{1}{2z\sqrt{1-1/z}}\ln\left(\frac{\sqrt{1-1/z}-1}{\sqrt{1-1/z}+1}\right), \tag{B8}$$

and $\Pi^{(1),v}$ is the well-known two-loop correction to the vacuum polarization [55] in the convention of [56]. The functions s_i in Eqs. (B2)–(B7) are constant as $z \to 0$ and only diverge logarithmically as $z \to \infty$.

[1] N. Kauer and G. Passarino, J. High Energy Phys. 08 (2012) 116.
[2] F. Caola and K. Melnikov, Phys. Rev. D **88**, 054024 (2013).
[3] J. M. Campbell, R. K. Ellis, and C. Williams, J. High Energy Phys. 04 (2014) 060.
[4] C. Englert and M. Spannowsky, Phys. Rev. D **90**, 053003 (2014).
[5] C. Englert, Y. Soreq, and M. Spannowsky, J. High Energy Phys. 05 (2015) 145.
[6] J. M. Campbell, R. K. Ellis, and C. Williams, Phys. Rev. D **89**, 053011 (2014).
[7] M. Aaboud *et al.* (ATLAS Collaboration), Phys. Lett. B **786**, 223 (2018).
[8] A. M. Sirunyan *et al.* (CMS Collaboration), Phys. Rev. D **99**, 112003 (2019).
[9] D. de Florian *et al.* (LHC Higgs Cross Section Working Group), arXiv:1610.07922.
[10] J. S. Gainer, J. Lykken, K. T. Matchev, S. Mrenna, and M. Park, Phys. Rev. D **91**, 035011 (2015).
[11] A. Azatov, C. Grojean, A. Paul, and E. Salvioni, Zh. Eksp. Teor. Fiz. **147**, 410 (2015)][J. Exp. Theor. Phys. **120**, 354 (2015).
[12] M. Buschmann, D. Goncalves, S. Kuttimalai, M. Schonherr, F. Krauss, and T. Plehn, J. High Energy Phys. 02 (2015) 038.
[13] A. Azatov, C. Grojean, A. Paul, and E. Salvioni, J. High Energy Phys. 09 (2016) 123.
[14] M. Spira, A. Djouadi, D. Graudenz, and P. M. Zerwas, Nucl. Phys. **B453**, 17 (1995).
[15] R. Harlander and P. Kant, J. High Energy Phys. 12 (2005) 015.
[16] C. Anastasiou, S. Beerli, S. Bucherer, A. Daleo, and Z. Kunszt, J. High Energy Phys. 01 (2007) 082.
[17] U. Aglietti, R. Bonciani, G. Degrassi, and A. Vicini, J. High Energy Phys. 01 (2007) 021.
[18] J. Davies, R. Gröber, A. Maier, T. Rauh, and M. Steinhauser, Phys. Rev. D **100**, 034017 (2019).
[19] R. V. Harlander, M. Prausa, and J. Usovitsch, J. High Energy Phys. 10 (2019) 148.
[20] E. W. N. Glover and J. J. van der Bij, Nucl. Phys. **B321**, 561 (1989).
[21] F. Caola, J. M. Henn, K. Melnikov, A. V. Smirnov, and V. A. Smirnov, J. High Energy Phys. 06 (2015) 129.
[22] A. von Manteuffel and L. Tancredi, J. High Energy Phys. 06 (2015) 197.
[23] F. Caola, K. Melnikov, R. Röntsch, and L. Tancredi, Phys. Rev. D **92**, 094028 (2015).
[24] F. Caola, M. Dowling, K. Melnikov, R. Röntsch, and L. Tancredi, J. High Energy Phys. 07 (2016) 087.
[25] M. Grazzini, S. Kallweit, M. Wiesemann, and J. Y. Yook, J. High Energy Phys. 03 (2019) 070.
[26] K. Melnikov and M. Dowling, Phys. Lett. B **744**, 43 (2015).
[27] J. M. Campbell, R. K. Ellis, M. Czakon, and S. Kirchner, J. High Energy Phys. 08 (2016) 011.
[28] R. Gröber, A. Maier, and T. Rauh, J. High Energy Phys. 03 (2018) 020.
[29] S. Borowka, N. Greiner, G. Heinrich, S. P. Jones, M. Kerner, J. Schlenk, U. Schubert, and T. Zirke, Phys. Rev. Lett. **117**, 012001 (2016); **117**, 079901(E) (2016).
[30] S. Borowka, N. Greiner, G. Heinrich, S. P. Jones, M. Kerner, J. Schlenk, and T. Zirke, J. High Energy Phys. 10 (2016) 107.
[31] G. Heinrich, S. P. Jones, M. Kerner, G. Luisoni, and E. Vryonidou, J. High Energy Phys. 08 (2017) 088.
[32] J. Baglio, F. Campanario, S. Glaus, M. Mühlleitner, M. Spira, and J. Streicher, Eur. Phys. J. C **79**, 459 (2019).
[33] R. Bonciani, G. Degrassi, P. P. Giardino, and R. Gröber, Phys. Rev. Lett. **121**, 162003 (2018).
[34] J. Davies, G. Mishima, M. Steinhauser, and D. Wellmann, J. High Energy Phys. 03 (2018) 048.
[35] J. Davies, G. Mishima, M. Steinhauser, and D. Wellmann, J. High Energy Phys. 01 (2019) 176.
[36] X. Xu and L. L. Yang, J. High Energy Phys. 01 (2019) 211.
[37] J. Davies, G. Heinrich, S. P. Jones, M. Kerner, G. Mishima, M. Steinhauser, and D. Wellmann, J. High Energy Phys. 11 (2019) 024.
[38] J. M. Campbell, R. K. Ellis, E. Furlan, and R. Röntsch, Phys. Rev. D **90**, 093008 (2014).
[39] J. M. Campbell, R. K. Ellis, and G. Zanderighi, J. High Energy Phys. 12 (2007) 056.
[40] V. Costantini, B. De Tollis, and G. Pistoni, Nuovo Cimento A **2**, 733 (1971).
[41] S. Catani, Phys. Lett. B **427**, 161 (1998).
[42] M. Beneke and V. A. Smirnov, Nucl. Phys. **B522**, 321 (1998).
[43] B. Jantzen, J. High Energy Phys. 12 (2011) 076.
[44] P. Nogueira, J. Comput. Phys. **105**, 279 (1993).
[45] J. A. M. Vermaseren, arXiv:math-ph/0010025.
[46] K. G. Chetyrkin and F. V. Tkachov, Nucl. Phys. **B192**, 159 (1981).
[47] A. V. Smirnov, Comput. Phys. Commun. **189**, 182 (2015).
[48] S. Laporta, Int. J. Mod. Phys. A **15**, 5087 (2000).
[49] See Supplemental Material at http://link.aps.org/supplemental/10.1103/PhysRevD.100.114013 for a Mathematica file containing the coefficients in the threshold expansion.
[50] M. Beneke, J. Piclum, and T. Rauh, Nucl. Phys. **B880**, 414 (2014).
[51] J. Fleischer and O. V. Tarasov, Z. Phys. C **64**, 413 (1994).
[52] P. Masjuan and S. Peris, Phys. Lett. B **686**, 307 (2010).
[53] B. Agarwal, *HXSWG Offshell and Interference Meeting* (2019), https://indico.mpp.mpg.de/event/6400/.
[54] B. Agarwal and A. von Manteuffel (to be published).
[55] A. O. G. Källén and A. Sabry, Kong. Dan. Vid. Sel. Mat. Fys. Med. **29**, 1 (1955).
[56] Y. Kiyo, A. Maier, P. Maierhöfer, and P. Marquard, Nucl. Phys. **B823**, 269 (2009).